NEW PROTECTION CONCEPTS FOR METEOROID / DEBRIS SHIELDS

K. Thoma, M. Wicklein, E. Schneider

Fraunhofer-Institute for High Speed Dynamics – Ernst-Mach-Institut, Freiburg, Germany, Email: thoma@emi.fhg.de

ABSTRACT

Manned space missions demand advanced safety requirements concerning protection against space debris and meteoroid impacts which lead to heavy shielding structures. In order to decrease the weight of shield systems without compromising the protection performance, or in order to increase protection levels at constant weight, modern shield concepts have been evaluated by means of experimental and numerical impact simulations. New configurations have been compared with existing "Stuffed Whipple Shield" protection systems. Such systems consist of an Al-bumper and a so-called "stuffing layer" consisting of a combination of ceramic and aramid fabrics. Results are presented for Al-foam sandwich bumpers and bumpers of TiAl super alloys. A number of materials have been implemented as stuffing layers: Kevlar fabrics, Nextel fabrics combined with Kevlar fabrics, and Kevlar fabrics combined with polyurethane foam. Numerical simulations are carried out for the Al-foam shields. These calculations are conducted mesomechanically, i.e. the cell walls of the foam are modelled explicitly with a finite element mesh. The aim is to study the influence of the foam on the distribution of momentum of the debris cloud.

1. INTRODUCTION

Increasing awareness of the space debris threat has lead to the development of relatively accurate and well established micrometeoroid and debris flux models (e.g. Kessler et al., 1978 and 1985). The relevance of these flux models has been confirmed following extensive analysis of impact damages on retrieved spacecraft components. Prominent examples are components of the Hubble Space Telescope and surfaces of the Space Shuttle (Hempsell, 1994; Christiansen, 1998; Bernhard et al., 1997). Debris environment population projections (e. g. Bendisch and Wegener, 2001) predict an essential population increase, independent of the scenario used (Fig. 1).

The purpose of this paper is to review current protection systems used for manned spacecraft (e.g. ISS), and to demonstrate new concepts offering enhanced protection capabilities.

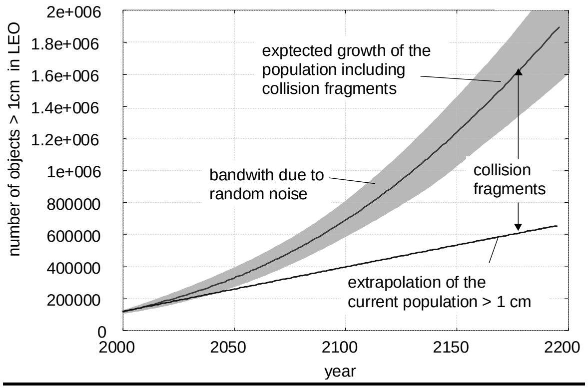

Figure 1. The principal growth of the future debris population > 1 cm in LEO (Bendisch and Wegener, 2001)

2. METEOROID / DEBRIS SHIELDS USED ON ISS MODULES

In unmanned spacecraft the requirements for orbital debris protective measures can usually be met by applying simple bumper shields which are spaced at a distance limited by launcher constraints. The safety requirements for manned missions are higher and therefore demand heavier shielding. To achieve higher performance, intermediate bumper layers can be placed between the bumper plate and primary structure.

Shields with intermediate layers of Kevlar (Aramide weave layers) and Nextel (ceramic fabric) – so-called "Stuffed Whipple Shields" – showed sufficient performance to be used to protect US modules on the International Space Station / ISS (Christiansen et al., 1995, and 2001).

In parallel to the development of the NASA Stuffed Whipple Shield, NASDA (Shiraki and Noda, 1998) and ESA (Destefanis et al., 1999) developed a similar type of heavy protection shields for their ISS modules.

The final solution for the ESA COLUMBUS Module was a Stuffed Whipple Shield configuration with an Al bumper and a combination of Nextel fabric and a Kevlar / Epoxy composite as intermediate layers (Schäfer, 1997). Instead of Aramide fabric layers used for the US modules the Kevlar composite plate is used for the COLUMBUS shield. A comparison of the NASA and

Proceedings of the Fourth European Conference on Space Debris, Darmstadt, Germany, 18-20 April 2005
(ESA SP-587, August 2005)

Table 1. Comparison of the performance of NASA and ESA heavy Stuffed Whipple Shield configurations at 3 and 7 km/s, normal impact; d is the ballistic limit diameter of the impacting Al-sphere, m the corresponding mass.

Config. Ref.	Ref.	bumper	Stuffing (layers)	primary structure	Total AD [g/cm^2]	spacing [cm]	d [cm] (m [gr]) at 3 km/s	d [cm] (m [gr]) at 7km/s
NASA Lab Module	Christi-ansen, 1995,2001	0.19 cm Al 6061	6 Nextel 312 AF 62/ 6 Kevlar 710	0.48 cm Al 2219 T87	2.67	11.4	0.65 (0.4)	1.3 (3.2)
ESA Columbus (cyl. section)	Faraud, 2002	0.25 cm Al 6061	4 Nextel 312 AF 62/ Kevlar 129/Epoxy 6 mm	0.48 cm Al 2219 T851	3.2	13.0	1.35 (3.6)	1.5 (4.9)

ESA shield configurations concerning materials, dimensions and performances is given in Tab. 1.

3. NEW PROTECTION SHIELD CONCEPTS FOR MANNED SPACECRAFT

To improve and optimize meteoroid and debris shields for manned spacecraft, the European Space Agency funded the “Enhanced Space Debris Shields” technology program. The study began with a review of existing shielding systems that are offering high protection levels. In addition an assessment of new concepts and materials for potential use in shielding was made taking into account system level requirements and design aspects. As a result, the review of the high protection shielding systems showed that structural, thermal and operational requirements have a strong influence on the final shielding design and its subsequent mass (Destefanis et al., 2003; Schneider et al., 2004).

Considering such constraints, the enhancement activity was restricted to investigating:
(A) novel bumper concepts;
(B) novel stuffing concepts; and
(C) a hybrid configuration.

Among the most promising new bumper concepts to be investigated were:

- a novel structural concept consisting of a sandwich panel with Al-foam core and face-sheets of different thicknesses (termed "Al-foam sandwich bumper")
- use of γ-TiAl super alloy for the bumper plate

The stuffing concepts primarily involved testing of a combination of flexible non-metallic materials:

- Kevlar fabric (Kevlar KM 2D)
- 2.5 D Kevlar mattresses (from EADS)
- Nextel 312 AF 62
- Polyurethane foam

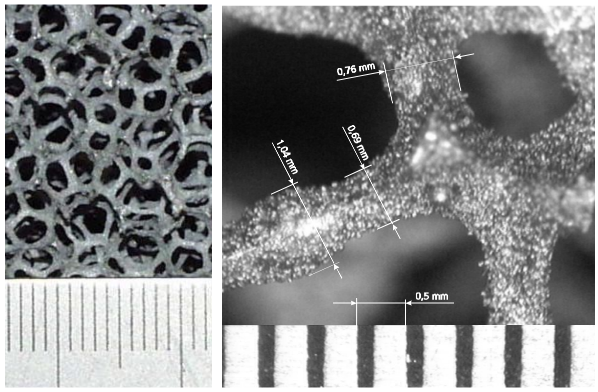

Figure 2. Open cell aluminum foam - close lookup (images refers to measurements made on 10 ppi foam)

The structure of the Al-foam used for the sandwich bumper is shown in Fig. 2.

Stuffing materials used for testing are displayed in Fig. 3.

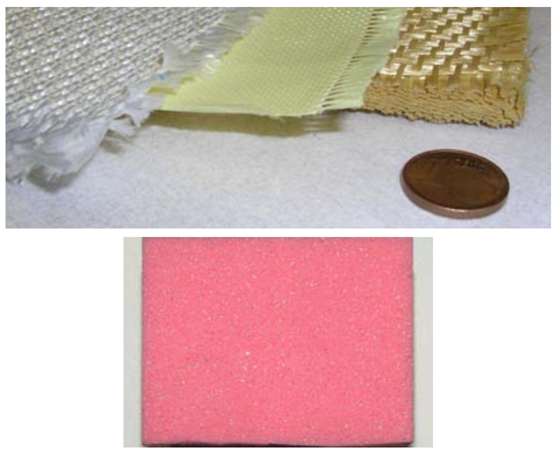

Figure 3. Nextel 312 style AF 62, Kevlar 2D, Kevlar 2.5D mattress, Polyurethane foam (Confor pink)

Table 2. Overview of configurations

Cfg.	External Bumper t* [mm] & type	Stuffing layers & type	Primary structure t [mm] and type	areal weight [g/cm²]
A1	2.0 Al6061, 40.0 20ppi Al-foam, 0.3 Al2024	-	4.90 Al2219	3.21
D2	1.76 γ-TiAl	4 Nextel / 33 Kevlar 2D	4.94 Al2219	3.21
D2mod	1.76 γ-TiAl	3 Nextel / 45 Kevlar 2D	4.95 Al2219	3.38
B1	2.6 Al6061	4 Nextel / 3 Kevlar 2.5D matr.	4.89 Al2219	3.28
B2	2.6 Al6061	4 Nextel / 33 Kevlar 2D	4.92 Al2219	3.22
B2mod	2.6 Al6061	3 Nextel / 45 Kevlar 2D	4.92 Al2219	3.38
B3	2.6 Al6061	4 Nextel / 40 mm PU / 15 Kevlar 2D	4.99 Al2219	3.24
AB2mod	2.6 Al6061, 30.0 20ppi Al-foam, 0.3 Al2024	25 Kevlar 2D	4.92 Al2219	3.42

* the thicknesses and areal weights are the actual values (not the nominal values). These values are averages if there have been more than one shot on the configuration

Tab. 2 presents an overview of the bumper and stuffing configurations indicating respective materials and dimensions. The areal weights given include the weight of the primary structure (module wall).

The COLUMBUS shield configuration given in Tab. 1 was taken as a reference to evaluate the test results.

Qualitatively, the following results have been obtained:

- γ-TiAl performs better as a bumper material than an equal areal weight Al-plate but bears a high risk of fracturing during impact
- the concept of an Al-foam sandwich bumper appears promising for high performance shielding although it may serve only as an additional fragmenter and therefore require an additional stuffing layer to act as a fragment catcher.
- polyurethane foam is not useful as a stuffing layer when sandwiched between a few layers of Nextel and Kevlar
- Kevlar 2.5 D mattresses have a slightly better protection performance than Kevlar 2D fabrics (however it is too expensive for industrial applications)
- Kevlar 2D is a high performance, energy dissipating, light-weight stuffing material even when used in a "stand-alone" configuration, i. e. without Nextel

Based on these findings configuration AB2mod has been identified as the preferred shield system. It combines several advantageous properties:

- high degree of projectile fragmentation due to multi-shock processes during perforation of the Al-foam sandwich bumper

- high structural stability of this bumper sandwich

- high stopping ability of behind bumper fragment/vapour clouds by multiple Kevlar 2D cloth layering taking advantage of the high yield strength of Kevlar

Different views of a AB2mod configuration test target are shown in Fig. 4.

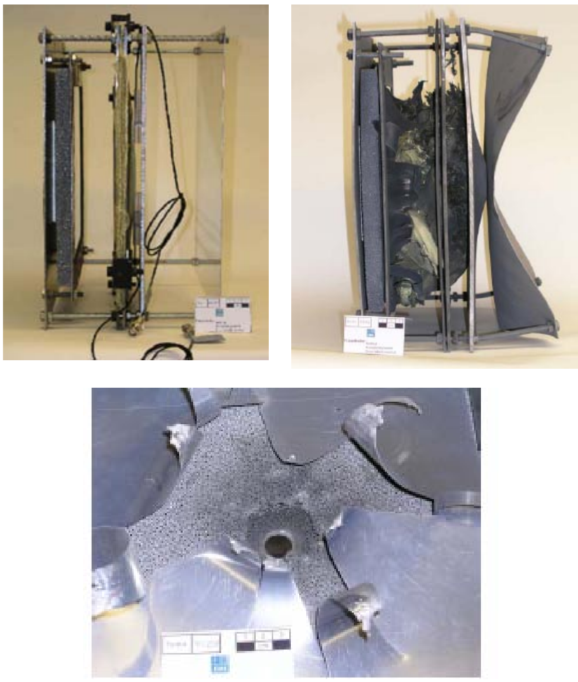

Fig. 4. Hybrid configuration "AB2mod"; top left: target before testing; top right: target after testing; bottom: rear view on impacted Al-foam sandwich bumper.

The AB2mod configuration has been experimentally tested in a wide range of impact velocities (about 2.5 km/s - 6 km/s) at different impact angles. Experimental

Table 3. *Test matrix and overview results for "hybrid" configuration AB2mod.*

Exp. No.	AD	Projectile					Result
		d	m	v	α	BL	
	[g/cm²]	[mm]	[g]	[m/s]	[°]		
10257	3.37	12.0	2.52	2527	0	<	craters (2.0); plate bulged (5x24)
10258	3.30	12.0	2.53	3036	0	<	craters (2.4); plate bulged (1.5x13)
10256	3.34	14.0	4.05	3107	0	>	perforation hole (21.6); plate bulged (6x5)
10153	3.42	15.0	4.97	5940	0	<	no craters; plate bulged (16x175)
10253	3.29	15.0	4.94	6369	0	<	no craters; plate bulged (16x160)
10152	3.41	14.5	4.49	6600	0	<	no craters; plate bulged (14x180)
10262	3.35	13.0	3.22	2960	45	<	craters (0.6); plate bulged (3.5x23)
10266	3.40	14.0	4.04	4428	45	<	craters (1.4); no bulge visible
10260	3.36	14.5	4.49	6425	45	<	craters (0.3); no bulge visible
10261	3.34	15.0	4.98	6539	45	>	craters (0.9); plate bulged (5x18)
10271	3.44	17.0	7.19	5900	60	<	craters (0.5); no bulge visible

parameters as well as ballistic limit and damage results are given in Tab. 3.

4. SIMULATION OF HVI ON ALUMINIUM FOAM

Based on the favourable experimental results for Al-foam, numerical simulations have been performed.

The mass specific stiffness of the material is comparable to aluminium honeycombs but the structure of the foam is isotropic, which results in the advantage that effects like ‘channeling’ do not occur when foam is used. In order to investigate the protection effect of an open-cell aluminium foam, 3D numerical simulations have been conducted at the Ernst-Mach-Institut, in addition to the hypervelocity impact tests. The simulations were done mesomechanically, i.e. the porous structure of the foam was modelled explicitly. For the simulations the adaptive code SOPHIA was used, which has been developed at Ernst-Mach-Institut. The purpose of the investigations was to identify the influence of projectile and foam parameters on the impact behaviour of the foam. The typical setup of the simulations is shown in Fig.5.

The aluminium foam (thickness 4 cm) is placed directly behind the bumper (aluminium, thickness 1.2 mm). When the projectile hits the bumper, a fragmentation cloud is created that can interact with the aluminium foam. This can lead to an additional lateral expansion of the fragmentation cloud. In order to quantify the lateral expansion, the momentum per area that is transferred to

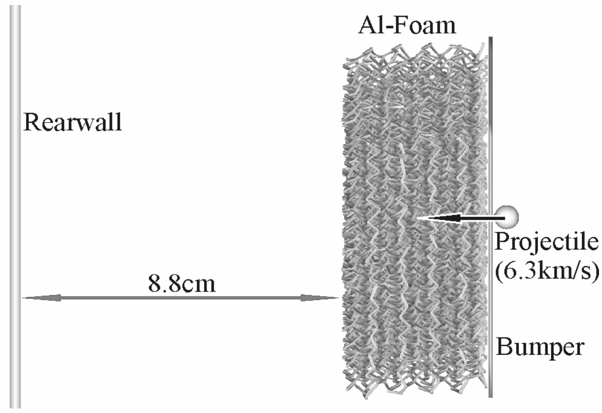

Figure 5. Hypervelocity impact on a Whipple-shield filled with an open-cell aluminium foam. The figure shows a typical finite element discretisation that was used in the numerical simulations.

the rear wall is calculated in the simulations, whereas only the component perpendicular to the rear wall is considered. The momentum distribution is evaluated in terms of the distance from the impact axis (only normal impacts have been considered). A typical result is shown in Figure 6.

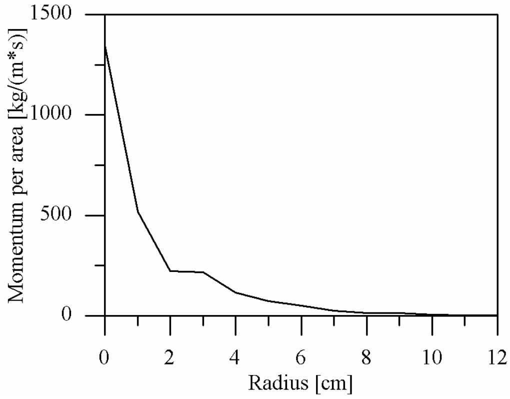

Figure 6. Radial distribution of the momentum per area transferred to the rear wall. The plot shows a typical result obtained for an impact as illustrated in Figure 5. The radius is the distance of an impacting fragment from the impact axis.

The maximum of the curve is at a radius of zero. Thus, the maximum damage of the rear wall is on the impact axis. This was confirmed in the experiments and in the simulations. In addition to the momentum distribution in terms of the radius, it is useful to define a scalar value representing the shape of the curve. This allows for the easy comparison of many different distribution curves. The lateral expansion E is defined as

$$E = \frac{\text{Momentum per area (4cm)}}{\text{Maximum momentum per area}} \qquad (1)$$

Thus, the momentum per area at a radius of 4 cm and at zero have to be determined. The expansion E of the curve in Figure 6 is 0.086 for example.

Wicklein et al. (2004) showed that the numerical simulations of the impacts on aluminium foam agree with the experimental observations. Therefore, in the following the focus will be on numerical investigations of the influence of projectile and foam parameters on the impact behaviour. For that purpose, a number of simulations have been done where the projectile velocity and its size have been varied as well as the cell size and the cell wall thickness of the foam. The failure criterion for the cell walls has been varied too. The variations were conducted with regard to a reference impact scenario. The parameters for the reference simulation were:

- Projectile radius: 3.45 mm
- Projectile velocity: 6.41 km/s
- Failure pressure of the cell walls: 800 MPa (tensile)
- Cell wall thickness: 0.68 mm
- Cell size: 8.36 mm

The cell sizes given in this work are a little larger than the average inner pore diameter but proportional to it. For the variations all parameters except one were kept constant. Only cell wall thickness and cell size were varied simultaneously to ensure that the areal density of the foam did not change. The ranges of the varied parameters were:

- Projectile radius: 2.3 mm – 10.35 mm
- Projectile velocity: 3 km/s – 15 km/s
- Failure pressure: 200 MPa – 10 GPa
- Cell wall thickness: 0.42 mm – 1.03 mm
- Cell size: 5.02 mm – 11.7 mm

Most of the calculations have also been executed for the case of a massive aluminium plate placed 4 cm behind the bumper having the same areal density as the foam. Thus, the efficiency of the foam could be analysed.
Fig. 7 illustrates the influence of the projectile radius on the lateral expansion of the fragmentation cloud.

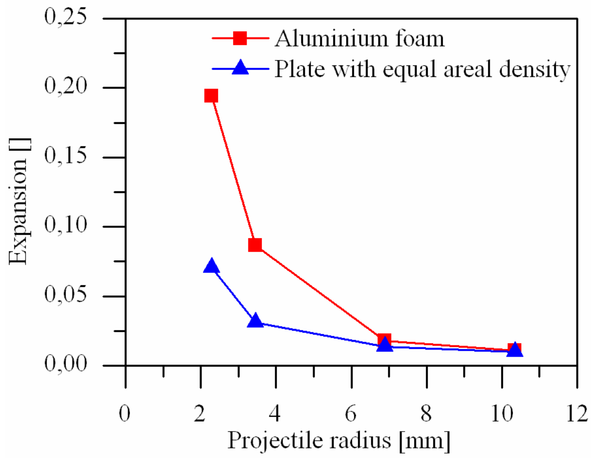

Figure 7. Expansion of the fragmentation cloud hitting the rear wall depending on the radius of the projectile. The results for impacts on a plate with the same areal density instead of the foam are also presented.

The expansion decreases fast with increasing projectile size. This is true for the foam and the plate. For small projectiles the expansion is much better in case of the foam. For a projectile radius of 10.35 mm the values for foam and plate are almost identical. In this case the diameter of the projectile is roughly twice as large than the average cell size of the foam. Note that the foam will 'look' more and more like a homogeneous continuum compared to the projectile the larger the projectile is. Therefore, the foam with its heterogeneous structure can only expand the fragmentation cloud effectively when the diameter of the projectile is smaller than the cell size of the foam.

The effect of a varying projectile velocity on the expansion is displayed in Fig. 8

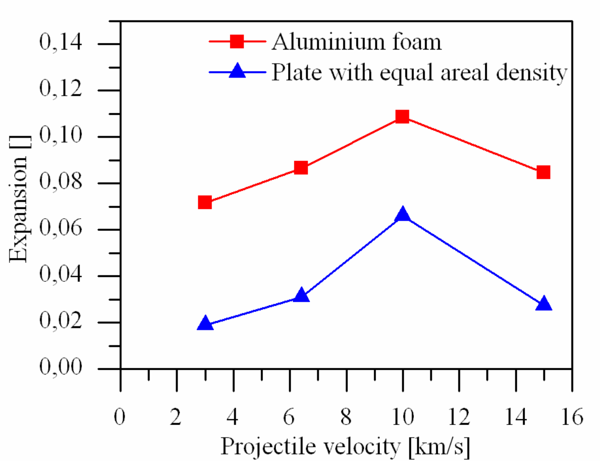

Figure 8. Influence of the projectile velocity on the expansion of the fragmentation cloud. In addition to the results of the impacts on the foam, a massive aluminium plate with equal areal density has also been considered.

For all velocities investigated the performance of the foam is superior to that of the plate. In both cases the expansion reaches a maximum at 10 km/s. The reason for this is not clear at the moment. Fig. 9 compares cross-sections of the foam samples after the impact event for projectile velocities of 3 km/s (lowest expansion) and 10 km/s (highest expansion).

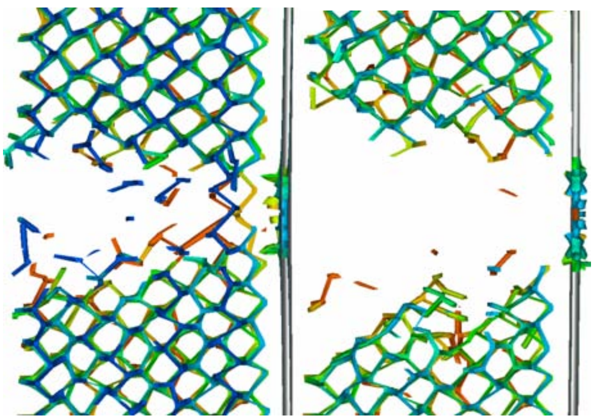

Figure 9. Cross-sections of foam samples after the impact for different projectile velocities. The velocities were 3 km/s (left) and 10 km/s (right).

Evidently, the damaged area at 10 km/s is much larger than for the low velocity in agreement with a higher lateral expansion. As the maximum of the expansion is also observed when the plate is applied (Fig. 8), the maximum is not an effect of the foam. But, as proofed by Fig. 8 the foam yields an additional expansion effect for all velocities.

In the simulations, failure of material is assumed to occur when the hydrostatic pressure within a finite element becomes larger than a value $p_{failure}$, which is always positive corresponding to a tensile stress state. If this occurs for a finite element, it is transformed into a particle that carries the momentum of the element but has no strength anymore. The particle can still interact with other elements and cause further failure of cell walls in the foam. Fig. 10 illustrates the influence of the failure pressure on the expansion of the fragmentation cloud.

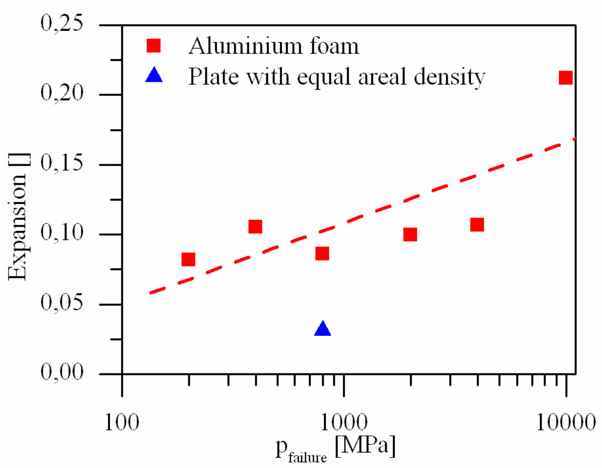

Figure 10. Expansion of the fragmentation cloud depending on the failure pressure of the cell walls in the simulations. Note that a logarithmic scale is used.

In these simulations, only the failure pressure of the foam material was varied. Fig. 10 reveals that the expansion rises when the cell walls become stronger. Although the failure pressure is varied over almost two orders of magnitude, the dependency is relatively weak. The dashed line represents the fit curve when a linear relationship between expansion and logarithmic failure pressure is assumed. On the other hand one could also interpret the data in such a way that the expansion is almost constant up to a failure pressure of 4 GPa.

Finally, the cell sizes and the cell wall thicknesses of the foam have been varied. For better comparability both parameters were varied such that the areal density of the foam samples was the same in all simulations. Due to this constraint not all combinations of cell size and cell wall thickness are possible. Thus, the thickness of the foam was varied too. But even so arbitrary combinations of the two parameters could not be realised with the used discretisation approach. Two examples of simulated foams with different cell size and cell wall thickness are pictured in Fig. 11.

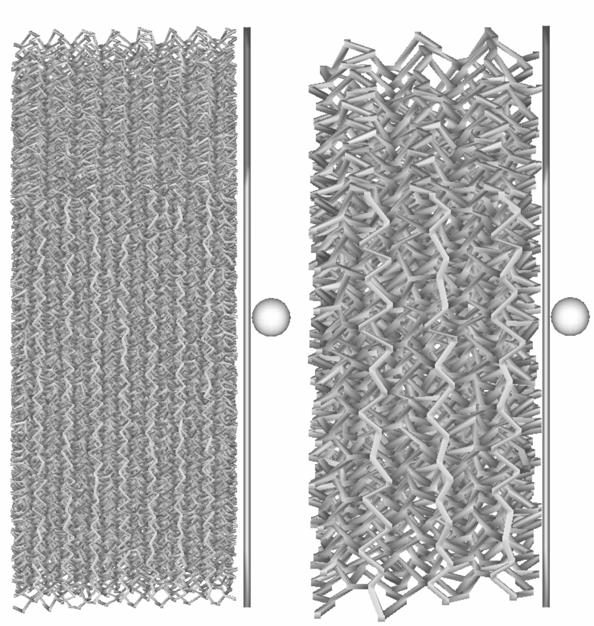

Figure 11. Foam discretisations with different cell wall thicknesses and cell sizes. The areal density of the foams is the same in both cases .

The calculated expansion of the fragmentation cloud is shown in Fig. 12 for the parameter combinations considered.

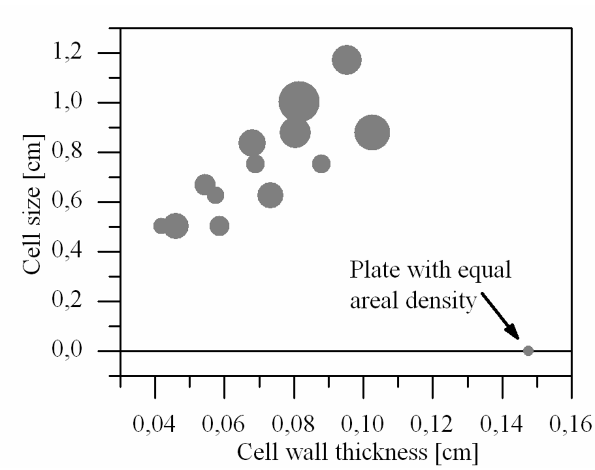

Figure 12. Dependency of the expansion on the cell size and cell wall thickness of the foam. The expansion E is represented by the radius of the circular areas.

For each simulation a circular area is given in the 2D parameter space of cell size and cell wall thickness. The expansion is proportional to the radius of the circular area. In addition to the foam results the value for the plate is also indicated. As the plate does not consist of cells, the cell size is set to zero in this case. The cell wall thickness is equated with the thickness of the plate. The expansion of any considered parameter combination for the foam is better than for the plate. Unfortunately, a clear tendency of how the expansion depends on cell wall size and cell wall thickness can not be observed.

From the numerical results presented above it can be concluded that the protection effect of aluminium foam against hypervelocity impact is better than that of an aluminium plate with the same areal density. In addition the foam offers much higher flexural stiffness. Furthermore, the protective performance of the foam increases with decreasing projectile size and reaches a maximum at 10 km/s.

5. CONCLUSIONS

- New advanced shielding concepts involving a variety of bumper and stuffing materials for manned spacecraft have been established and investigated experimentally as well as numerically.

- A so-called hybrid shield configuration, consisting of an Al-foam sandwich bumper and a multi-layer Kevlar 2D intermediate stuffing, has been identified as best solution. It combines high structural stiffness with a high degree of projectile fragmentation and considerable fragment energy dissipation.

- The experimentally observed favourable behaviour of the Al-foam bumper system has been fully confirmed by the numerical results.

- Based on the "Al-foam Sandwich bumper" that was thoroughly investigated in this study, a whole class of new and effective shielding systems for manned spacecraft and structure walls of satellites can be developed.

6. ACKNOWLEDGEMENT

This work has been supported by **Deutsche Forschungsgemeinschaft** and was partly funded under **ESA Contract** 15512.

7. REFERENCES

Kessler D. J. and Cour-Palais B. G., Collision Frequency of Artificial Satellites: The Creation of a Debris Belt, *Journal of Geophysical Research,* 83 (A6), 1978.

Kessler D. J. and Su S. Y., Orbital Debris, *NASA-CP-2360*, March 1985.

Hempsell M., Hubble Array Impacts, *Spaceflight* 36, 1994.

Christiansen E. L., Orbiter Meteoroid/Orbital Debris Impacts: STS-50 (6/92) through STS-86 (10/97), NASA Johnson Space Center JSC-28033, August 1998.

Bernhard R. P., Christiansen E. L. and Kessler D. E., Orbital Debris as Detected on Exposed Spacecraft Surfaces, *Int. J. Impact Engng.*, Vol. 20, 111-120, 1997.

Bendisch J. and Wegener P., Analysis of Debris Mitigation Scenarios in Terms of Cost and Benefit, *Proceedings of the Third European Conference on Space Debris*, ESOC, Darmstadt, Germany, 19-21 March 2001.

Christiansen E., Crews J., Williamsen J., Robinson J., Nolen A., Enhanced Meteoroid and Orbital Debris Shielding, *Int. J. Impact Engng.*, Vol. 17, 217-228, 1995.

Christiansen E. L., Kerr J. H., Ballistic Limit Equations for Spacecraft Shielding, *Int. J. Impact Engng*., Vol. 26, 93-104, 2001.

Shiraki K., Noda N., Evaluation of Space Station JEM MM-OD Shield and Structural Design, IAF-98-I.5.07, *49th International Astronautical Congress*, Melbourne, Australia, September 28-October 2, 1998.

Destefanis R. et al., Columbus Debris Shielding Experiments and Ballistic Limit Curves, *Int. J. Impact Engng.*, Vol. 23, 181 - 192, 1999.

Schäfer F., Hypervelocity Impact Test Campaign, Columbus APM-COF Phase 2 - Report No. 1, Contract No. APRV/AR95/0025 Extension, Report No. EMI-HVITC-003, Fraunhofer EMI, Freiburg, Germany, October 31, 1997.

Faraud M., Destefanis R., MDPS Design Analysis and Damage Model Standards, Alenia Report No. COL-RP-AI-0106 Issue 4, Alenia Spazio, Torino, March 1, 2002.

Destefanis R., Schäfer F., Lambert M., Faraud M., and Schneider E., Enhanced Space Debris Shields for Manned Spacecraft, *Int. J. Impact Engng*. Vol. 29, 213-226, 2003.

Schneider E., Schäfer F., Destefanis R., and Lambert M., Advanced Shields for Manned Space Modules, IAC-04-IAA.5.12.01, *55th International Astro-nautical Congress,* Vancouver, Canada, 2004.

Wicklein M., Hiermaier S., Thoma K., Simulation of Cellular Aluminium: Crash and Impact, *Proceedings of the symposium "Cellular Metals and Polymers*", Fürth, Germany, 12.-14. October 2004.